Influence of chemical effects on Al high resolution Kα X-ray spectra in proton and alpha particle induced X-ray spectra

Stjepko Fazinić [a], Iva Božičević Mihalić*[a], Anja Mioković [a], Mauricio Rodriguez Ramos[†a], Marko Petric[b,c]

a) Ruđer Bošković Institute, Bijenička cesta 54, 10000 Zagreb, Croatia
b) Faculty of Geotechnical Engineering, Hallerova aleja 7, 42000, Varaždin, Croatia
c) Jožef Stefan Institute, Jamova 39, 1000 Ljubljana, Slovenia

*Corresponding author: Iva.Bozicevic.Mihalic@irb.hr
[†]Present Address: Centro Nacional de Acelerados (U. Sevilla, CSIC, J. de Andalucia), 41092 Seville, Spain.

Abstract

Kα x-ray emission induced by 2 MeV protons and 3 MeV He ions in thick pelletized Al metal, Al_2O_3, Al_2S_3, AlN, $AlPO_4$ was measured using wavelength dispersive spectrometer with flat diffraction crystal to study the chemical sensitivity of related X-ray spectra. The energy shifts and relative intensities of of $K\alpha L^1$ multiple ionization satellites were determined for proton excitation. For He excitation we were able to study $K\alpha L^1$, $K\alpha L^2$ and $K\alpha L^3$ multiple ionization satellite components of Al Kα spectra. Intensity ratios of two major $K\alpha L^1$ components ($K\alpha_3$ and $K\alpha_4$) were determined for both 2 MeV proton and 3 MeV He excitations. Relative intensities of Kα diagram lines ($K\alpha L^0$) and $K\alpha L^1$, $K\alpha L^2$ and $K\alpha L^3$ multiple ionization satellites were determined for 3 MeV He excitation. The energy shifts of $K\alpha_{1,2}$ and multiple ionization satellite (MIS) peaks were determined using the spectra obtained from the Al and Al compounds mixed with MgBr, where Br Lα and Lβ peaks were used as internal calibration standards. The results confirm statistically relevant energy shifts for Al $K\alpha_{1,2}$ X-ray peaks from the measured compounds. The Al $K\alpha_{1,2}$ energy shifts show linear decrease with the increase of the calculated effective charge on Al atoms. Similar linear dependance of the peak energy shift vs. the effective charge on Al atoms have been observed on $K\alpha L^1$ multiple ionization satellite components Kα' and $K\alpha_4$ measured by 3 MeV He excitation

Introduction

It is well known that the fine structure of characteristic X-rays emitted from an atom depends on the chemical bonds between that element and the surrounding atoms. The influence of such chemical effects on X-ray emission spectra has been extensively studied over the decades to provide information about bonding to the nearest neighbouring atoms and as a tool for chemical speciation [1]. Most experimental studies are concentrated on K X-ray band, including energy shifts and intensity ratios of various X-ray line components [2-12]. The effects are in general larger for Kβ X-ray band compared to Kα X-rays [13-18]. However, in case of lighter elements like Mg, Al or Si, Kβ X-ray intensities relative to Kα are very low for practical laboratory applications. Most studies on Al K X-rays have been concentrated on the comparison of aluminium and aluminium oxide (Al_2O_3) spectra, focusing mostly on Al Kα [19-30] and to a lesser extent on Al Kβ regions [19-22, 31, 32]. Most studies were focused on Kα and/or Kβ energy shifts. In addition, relative intensities of different multiple ionization satellite (MIS) lines have also been studied [29, 30, 33, 34].

In general, the process of X-ray emission can be seen as a two-step process in which the relaxation of the K shell ionized atom can be seen as independent of the mode of excitation. Excitation is usually performed by photons using X-ray generators or synchrotron accelerators (X Ray Fluorescence - XRF), then low energy electrons (Electron Probe Micro-Analysis or EPMA) or low energy ion beams (Particle Induced X-Ray Emission or PIXE). Irrespective of the excitation mode multi vacancy states can be created. De-excitation of such states results with the MIS lines that can be observed with high resolution X-ray spectrometers at the energies slightly above the respective parent lines resulting from de-excitation of single-vacancy states. In case of K X-rays, such satellite lines are usually denoted as KL^i, where i is the number of L spectator vacancies created. MIS relative intensities depend on the mode of excitation. In case of charge particle ionization, the Coulomb interaction provides additional ionization mechanism to the ''shake'' process [35] characteristic for photon excitation. In case of charged particle ionization MIS relative intensities depend on the ions used and their energy. On the other hand, energies of individual lines and their shifts should in principle be independent of the excitation mode.

Baun and Fischer proposed to use the intensity ratios of $K\alpha L^1$ components α_4 and α_3 to $K\alpha_{1,2}$ as a test of oxidation on metallic targets [36]. Several papers reported relative intensities of the α_4 and α_3 satellite peaks in Al and its compounds induced by photons [27-29], electrons [20, 22] and ions [24, 33, 37]. Cureatz et al. [38] recently demonstrated the influence of multiple ionization satellites induced by 3-5 MeV energy He ions on the accuracy of He induced PIXE used with the standard SDD Energy Dispersive detectors. In that work, high resolution Wavelength Dispersive Spectrometer was used to study the fine structure of Kα X-rays induced by He ions for the range of elements from P to Cr, following the work of Heirwegh et al. [34, 39] on Mg, Al and Si, including their oxides.

In this work, we extend their work to study the fine structure of Al Kα X-rays in selected Al compounds excited with 2 MeV protons and 3 MeV He ions, with the goal to determine energy shifts and relative intensities of individual X-ray lines, including Kα MIS components, for Al metal and selected Al compounds.

Materials and methods (Experimental)

For the present experiment we used compressed pellets made up of high purity powders obtained from Sigma Aldrich Co., Inc., Milwaukee., WI, USA. The following targets were irradiated: Al, Al_2O_3, Al_2S_3, AlN and $AlPO_4$.

The High Resolution PIXE measurements were performed using our high resolution flat crystal spectrometer installed at the ion microprobe end-station of the Ruđer Bošković Institute Tandem Accelerator Facility in Zagreb. Detailed description of the spectrometer and an explanation of the X-ray spectra extraction algorithm can be found elsewhere [40, 41], and therefore only basic data are given here. The spectrometer consists of a sample holder, flat diffraction crystal and CCD X-ray detector enclosed in the vacuum chamber and mounted behind the main ion micro beam chamber. A schematic view is presented by Fazinić et al. [40] in Figure 2. The ion beam focused to about 10 µm in diameter hits the target and as a result characteristic X-rays are emitted and diffracted from the diffraction crystal to the CCD. The distance between the ion beam position on the target and the position on the CCD where the diffracted X-ray is detected varies between ≈ 55–66 mm, and the distance between the CCD plane and the diffraction crystal can be selected between ≈ 15–90 mm depending on the X-ray energy of interest.

The X-rays from the samples diffracted from a flat ADP (101) diffraction crystal were detected by a thermoelectrically cooled 1056x1027 channel CCD camera with 13 x 13 µm^2 pixel size. The influence of the Ion beam induced luminescence (IBIL) in some targets, which causes a background noise in the CCD detector, was eliminated with the addition of 1 µm thick graphite-coated Mylar foil (with ≈ 1 µm thick graphite layer) in front of the CCD.

Altogether three independent measurements were performed: (i) At first the compressed pellets prepared from the Al compound powders mixed with high purity MgBr obtained from the same supplier were irradiated with a 2 MeV proton beam; (ii) then pure compressed pellets of Al compound powders were irradiated with 2 MeV protons; and (iii) at the end the same pellets were irradiated with a 3 MeV He beam. In all the cases ion beam current was about 1 nA.

The first set of measurements was used to perform X-ray energy calibration following the procedure of Sato et al. [42]. We consider this step important for determination of Al Kα energy shifts. Related energy shifts documented in the available literature are at the values between 0.1 to 0.5 eV, which is very low and even the thermal stability of the spectrometer could have an influence on the results due to possible thermal expansion of the diffraction crystal plane distance, which could lead to the angular shift of the transition line peak position [19]. In our setup the spectrometer is placed in vacuum and we do not expect high temperature changes during individual runs. Anyhow, by performing the calibration measurements on the pellets mixed with MgBr we could use the Br Lα and Lβ X-ray peaks as internal calibration standard.

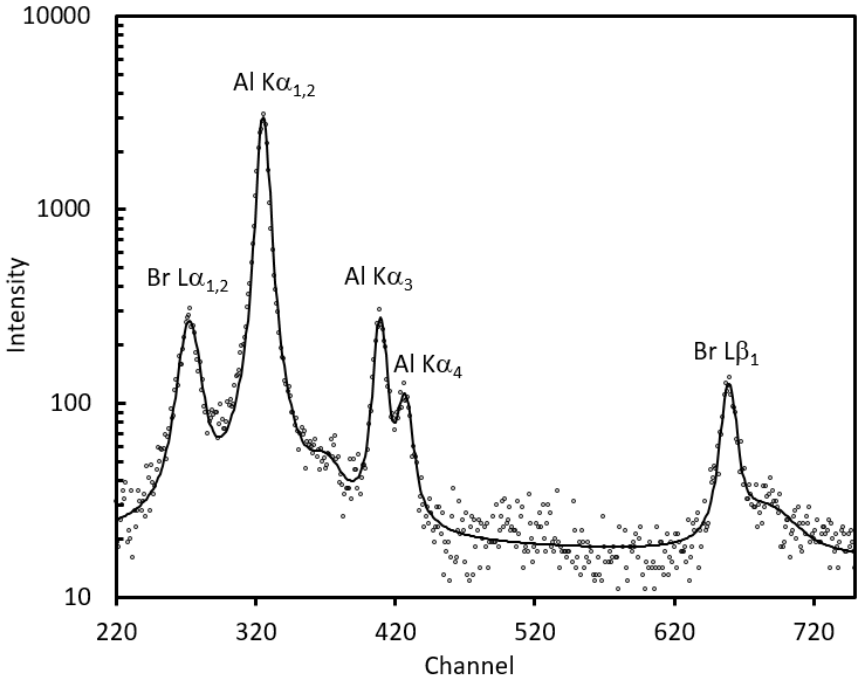

Figure 1. Relevant part of the Al Kα measured spectrum of an Al powder sample mixed with MgBr powder used for energy calibration.

Figure 1 shows the relevant region of the spectrum related to the mixed Al+MgBr target, used to start the calibration procedure. In addition to $K\alpha_{1,2}$ doublet, the spectrum clearly shows Al $K\alpha_3$ and $K\alpha_4$ components and two Br X-ray peaks: $L\alpha$ and $L\beta_1$. These two last peaks have been used as reference points for all the measured mixed spectra since they will remain at the same relative positions for all the measured spectra. In the calibration we used the fact that

$$\sin\theta = \frac{z}{\sqrt{z^2 + (t + channel \cdot 13)^2}} \qquad (1)$$

where θ is Bragg diffraction angle, (z/2) is the distance between the CCD plane and the diffraction crystal expressed in μm, t is the distance between the ion beam position on the target and the position of the zero channel on the CCD, channel corresponds to the pixel on the CCD where the diffracted X-ray is detected. Number of channels is 1056 and the each one has a width of 13 μm, which is the same as the CCD pixel size. Since sin θ = nλ/2d, where λ is the X–ray wavelength, d is the ''grating constant' of the crystal and n is the order of diffraction, and taking in account that the X-ray energy E equals to hc/λ (h is Planck constant and c is speed of light) the final relation between the X-ray energy and the channel in the related recorded spectrum is

$$E = \frac{nhc}{2d}\sqrt{1 + \left(\frac{t + channel \cdot 13}{z}\right)^2} \qquad (2)$$

The calibration procedure started with the mixed Al+MgBr spectrum. From the measured spectrum we extracted first moments (M1) of Br Lα, Br Lβ1, Al $K\alpha_{1,2}$ and Al $K\alpha_3$ peaks. Definition for peak first moments can be found elsewhere [43]. In this case the peak first moments were obtained using the channels having intensities larger than 50% of the maximum intensity. Then we used Deslattes et al. [44] experimental data for the Br Lα and Al $K\alpha_{1,2}$ X-ray peaks (1480.46 eV and 1486.57 eV respectively) to calibrate the spectrum. In such a way Br $L\beta_1$ energy was determined. Then the Br Lα and Br $L\beta_1$ peak energies were used as reference data to calibrate all the other measured spectra from Al compound targets mixed with MgBr.

The spectra obtained from pure Al compounds by both 2 MeV proton and by 3 MeV He ion excitations were calibrated using as the reference points the energies of Al $K\alpha_{1,2}$ and Al $K\alpha_3$ peaks determined from Al compound targets mixed with MgBr.

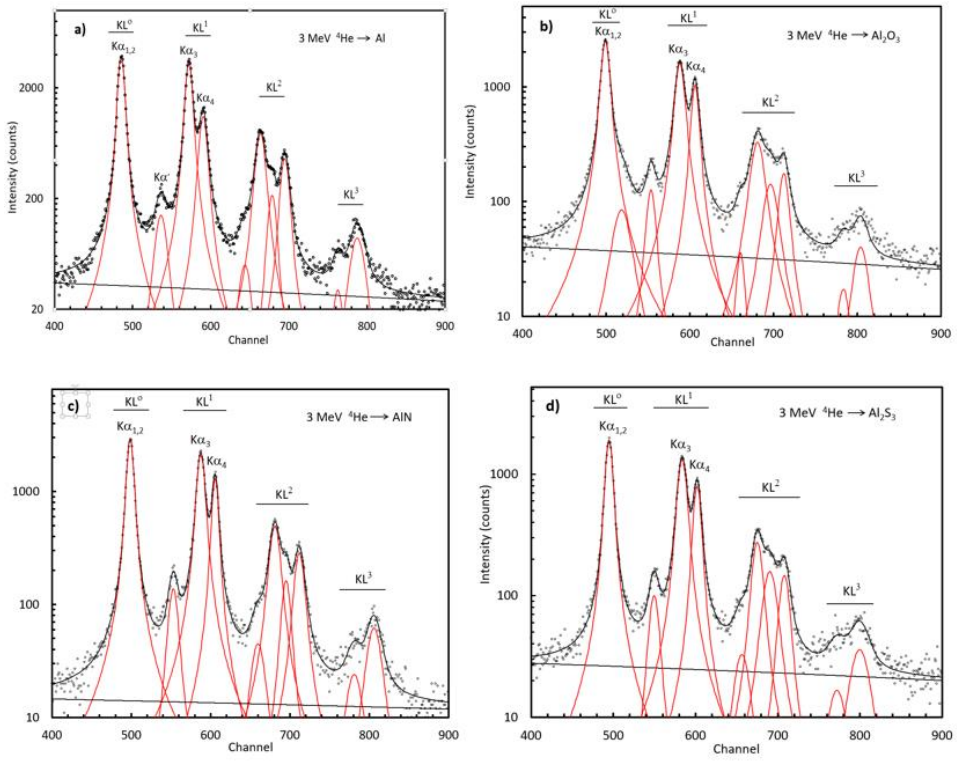

Figure 2. Measured spectra by 3 MeV ^{4}He excitation, showing the fitted lines and background models.

All the spectra from pure Al compounds excited with 2 MeV protons and by 3 MeV He ions were fitted and the peaks were modelled using Voigt functions with all free parameters (the linewidths, peak areas and peak centroids). A linear background was assumed to be an appropriate approximation for the small energy range concerned. In the process we introduced as many peaks as were necessary to minimize the fit residues and hence the reduced chi-squared values. An illustration of the fit procedure, Figure 2 shows the measured spectra of Al, Al_2O_3, AlN and Al_2S_3 under 3 MeV ^{4}He excitation, showing the fitted lines and background models.

Reported relative peak intensities extracted from the fitted spectra were corrected for X-ray attenuation through the graphitised Mylar foil and for geometrical effects. Cumulative corrections are negligible for $K\alpha_3$ to $K\alpha_4$ peak intensity ratios, while for calculation of relative intensities of KL^0 to KL^3 components excited by 3 MeV He ions, the correction factors are up to 2%.

Results and discussion

Figure 3 shows the $K\alpha_{1,2}$ region of all the measured pure Al compound spectra with 2 MeV proton excitation. For easier comparison, the spectra are normalized to the same $K\alpha_{1,2}$ centroid intensity. The energy shifts (determined from the samples mixed with MgBr) of the Al $K\alpha_{1,2}$ line are clearly seen for different compounds.

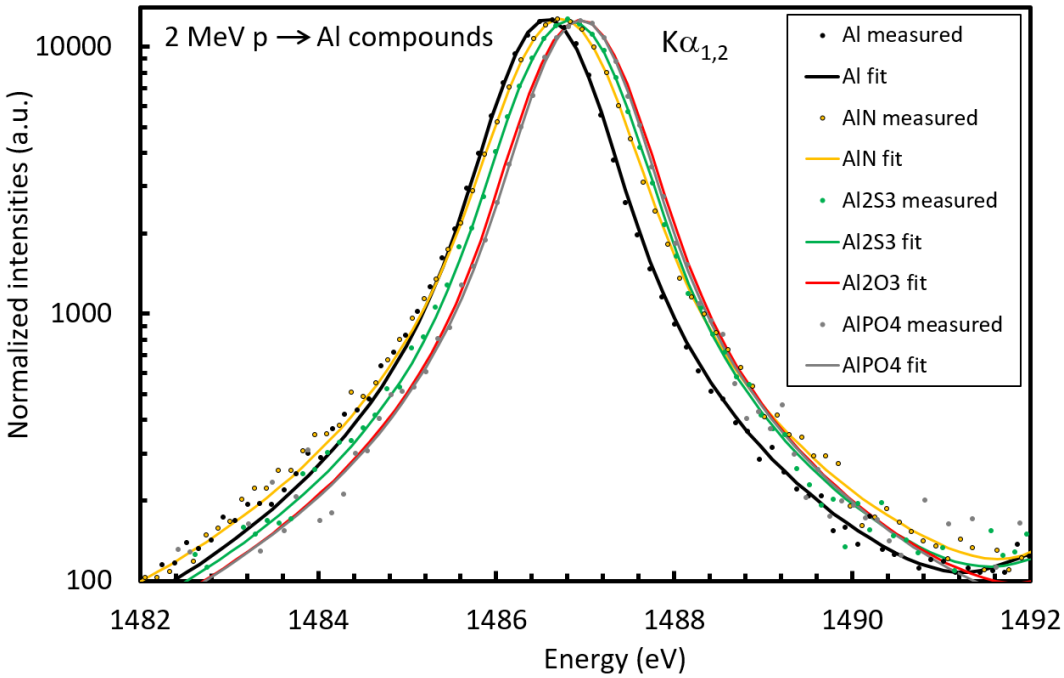

Figure 3. $K\alpha_{1,2}$ region of the spectra of all the measured Al compound samples by 2 MeV proton excitation, showing the energy shifts of the Al $K\alpha_{1,2}$ line.

Table 1. $K\alpha_{1,2}$ energy shifts determined from the samples mixed with MgBr for measured Al compounds and excitation by 2 MeV protons.

	Measured Kα1,2 M1 E shift (eV)	Literature data* (eV)	Reference
AlN	0.139 ± 0.032	0.293	[23]
		0.14	[19]
Al_2S_3	0.246 ± 0.033	0.276	[23]
Al_2O_3	0.360 ± 0.036	0.314	[23]
		0.39	[19]
		0.4	[24]
		0.4	[20]
		0.5	[45]
		-0.5	[27]
$AlPO_4$	0.376 ± 0.033		

*Energy shifts as reported in the literature, not necessarily related to M1 positions.

Table 1 shows tabulated Al M1 $K\alpha_{1,2}$ energy shifts from the present measurements together with the available data from literature. Energy shifts from the literature are not necessarily related to M1 positions. Most of the literature data can be found for Al_2O_3, where the reported energy shifts vary from +0.314 eV to +0.5 eV, with the exception of Suresh et al. [27] who reported negative energy shift (-0.5 eV). Most reported values refer to X-ray or electron beam excitation and none to proton or heavier ion excitation. Our measured energy shifts for Al_2O_3 and AlN are in very good agreement with the values reported by Anagnostopoulos et al. [19] obtained by X-ray excitation and in the case of Al_2S_3 with the data reported by Asada [23]. Measured energy shift for $AlPO_4$ is similar to the Al_2O_3, which is somehow expected since in both compounds Al is chemically bound to oxygen.

For third-row elements like phosphorus, sulphur, and chlorine the Kα1 emission energies are shifted to higher energies with the decrease of the effective charge on investigated atoms [46]. The change in electron density of valence electrons reduces the effective nuclear potential experienced by core electrons producing small energy shifts [47]. To investigate this mechanism as well for Al, the ab-initio calculations based on density functional theory (DFT) were performed. The initial crystal coordinates are taken from the Materials Project [48] and the crystal structure was relaxed by the cp2k software package [49]. The TZV2P-MOLOPT-SR-GTH and DZVP-MOLOPT-SR-GTH [50] basis sets were used for Al and all other atoms, respectively, along with Goedecker-Teter-Hutter pseudopotential [51]. The unknown exchange-correlation potential was substituted with Perdew-Burek-Ernzerhof (PBE) functional, parameterized for the solid and surface state [52]. On the optimized crystal structure, the Hirshfeld population analysis [53] was performed, yielding the effective charge for each atom within the crystal. The results for the studied Al compounds are presented in Figure 4. The obtained results are consistent with the measured energy shifts, confirming the energy shift decrease with the increase of the calculated effective charge on Al atoms, which is also consistent with the observations for the other third-row elements.

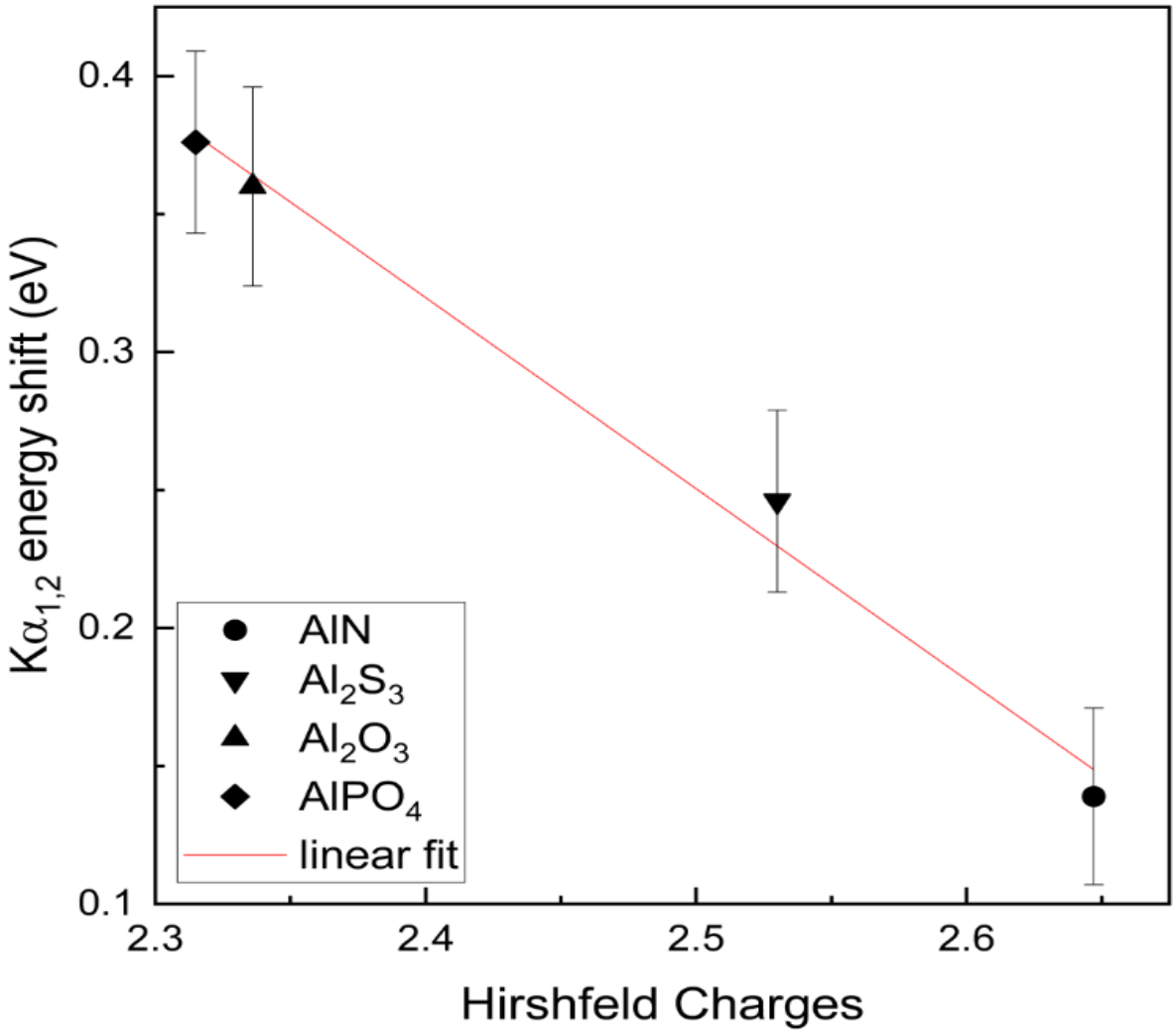

Figure 4. The experimental M1 $K\alpha_{1,2}$ energy shifts vs effective calculated charges on Al atom.

Figure 5 shows the $K\alpha L^1$ region of all the measured spectra with 2 MeV proton excitation. All the spectra are normalized to the same $K\alpha_{1,2}$ centroid intensity (as at Figure 3). Therefore, the figure demonstrates relative intensities (compared to $K\alpha_{1,2}$ peak) and energy shifts of Al $K\alpha L^1$ components, i.e. Kα', $K\alpha_3$ and $K\alpha_4$ X-ray lines.

Table 2. $K\alpha_3$ and $K\alpha_4$ energy shifts for measured Al compounds from 2 MeV proton excitation.

	$K\alpha_3$ M1 E shift (eV)	Literature* data (eV), excitation and ref	$K\alpha_4$ E shift (eV)
AlN	0.46 ± 0.10		0.46 ± 0.10
Al_2S_3	0.36 ± 0.14		0.51 ± 0.14
Al_2O_3	0.71 ±0.09	0.7 5 MeV He, [24] 0.6 electrons, [20] 0.9 X-rays, [45]	
$AlPO_4$	0.61 ± 0.07		0.70 ± 0.07

*Energy shifts as reported in the literature, not necessarily related to M1 positions.

Table 2 shows measured energy shifts for Al M1 $K\alpha_3$ and $K\alpha_4$ lines together with the available data from literature, only found for Al_2O_3 $K\alpha_3$ line. Our value for $K\alpha_3$ Al_2O_3 energy shift agrees well with the energy shift reported by Burkhalter et al [24] who used 5 MeV He ions for excitation. As previously explained, $K\alpha_3$ energy shift was determined from the spectra obtained from the samples mixed with MgBr, while the $K\alpha_4$ energy shift was determined from the spectra obtained from pure Al compounds. Intensities of Kα' are at the detection limit level and therefore we could not determine their energy shifts. However, the intensities of satellite peaks are much higher for He excitation. Therefore, we could use the spectra excited by 3 MeV He ions to extract energy shifts of Kα' and other lower intensity satellite components.

Figure 6 shows normalized Al spectra from all the measured Al compounds by 3 MeV He ion excitation. Energy calibration was performed using the $K\alpha_{1,2}$ and $K\alpha_3$ energies determined from 2 MeV proton measurements. As expected, intensities of satellite lines are much larger than in the case of proton excitation, including KL^2, KL^3 satellites, and enhanced Kα' line.

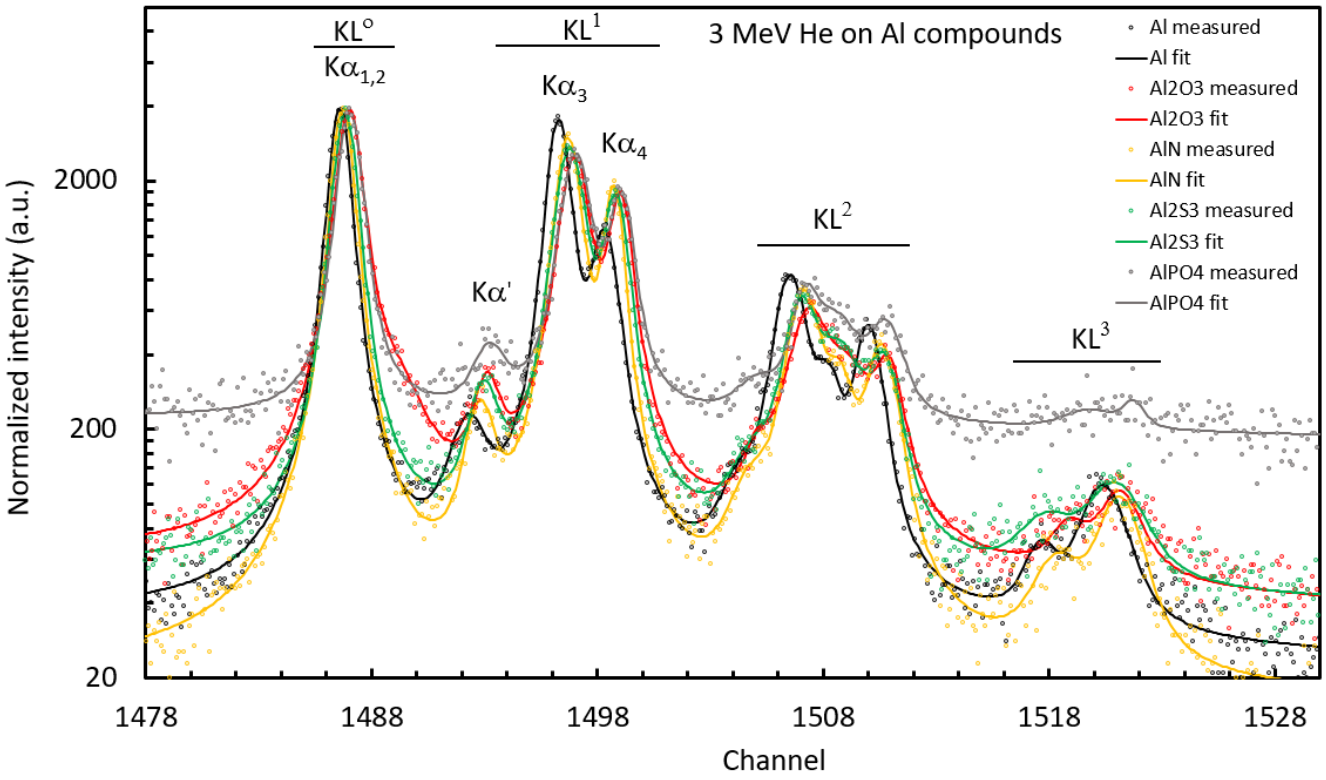

Figure 6. Normalized Al spectra obtained after 3 MeV He excitation.

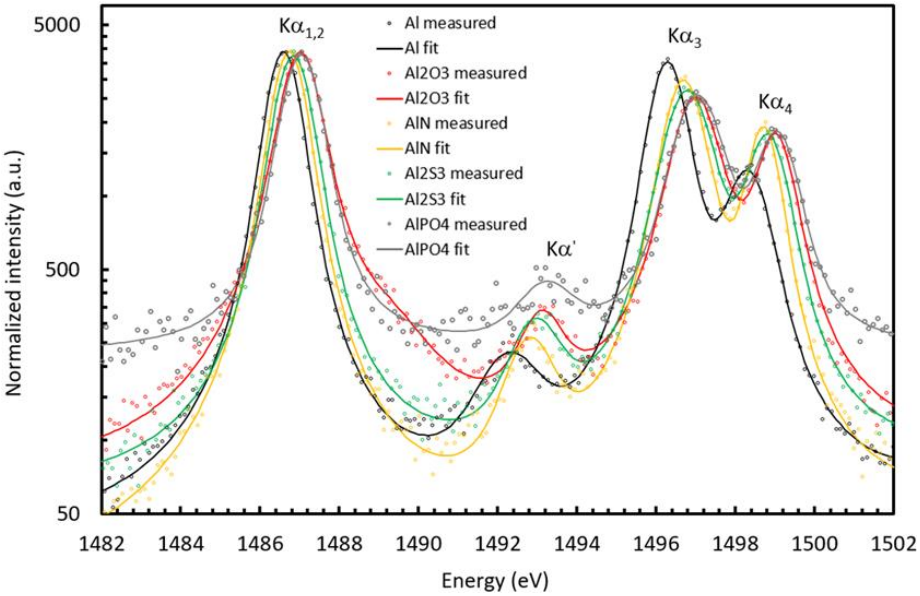

Figure 7. Normalized Al KL^0 and KL^1 regions of the Al spectra from the measured Al compounds excited by 3 MeV He ions.

The region of $K\alpha_{1,2}$, $K\alpha'$, $K\alpha_3$ and $K\alpha_4$ is enlarged in the Figure 7. The energy shifts of individual components and variations in $K\alpha_3$ and $K\alpha_4$ line intensities are clearly seen. Table 3 shows numerical values for Kα' and $K\alpha_4$ energy shifts obtained with 3 MeV ^{4}He excitation.

Table 3: Kα' and $K\alpha_4$ energy shifts (eV) obtained with 3 MeV ^{4}He excitation.

Al compound	Kα'	$K\alpha_4$
AlN	0.521 ± 0.084	0.393 ± 0.009
Al_2S_3	0.669 ± 0.080	0.499 ± 0.009
Al_2O_3	0.832 ± 0.080	0.697 ± 0.010
$AlPO_4$	0.93 ± 0.11	0.732 ± 0.012

Figure 8 shows the relationships between the experimentally determined Kα' and $K\alpha_4$ energy shifts and effective calculated charges on Al atom. Similar linear trends have been observed as for $K\alpha_{1,2}$ energy shifts observed by the excitation with 2 MeV protons (Figure 4).

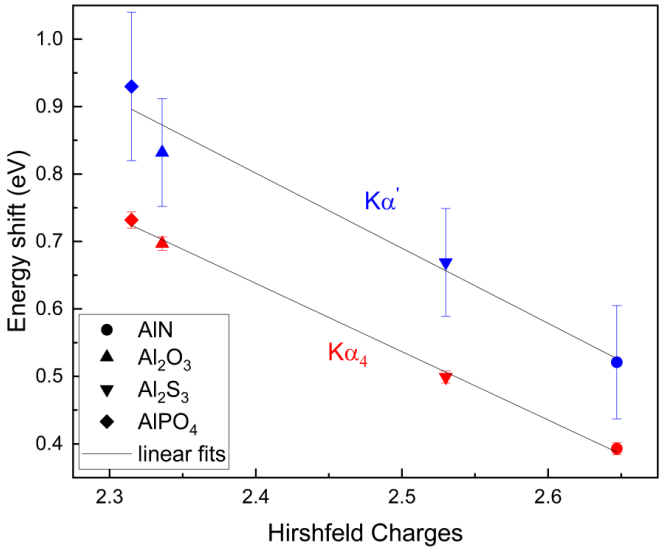

Figure 8: The experimental Kα' and $K\alpha_4$ energy shifts vs effective calculated charges on Al atom obtained with 3 MeV He excitation.

Table 4 shows numerical values for KL^i normalized intensities obtained with 3 MeV ^{4}He excitation, including for comparison $K\alpha_3$ to $K\alpha_4$ intensity ratios obtained by 3 MeV ^{4}He and by 2 MeV proton excitations. For 2 MeV proton excitation and our thick targets, KL^1 overall intensities relative to KL^0 are: 0.146 ± 0.004 for Al, 0.152 ± 0.002 for Al_2O_3, 0.150 ± 0.002 for AlN, 0.146 ± 0.003 for Al_2S_3, and 0.146 ± 0.004 for $AlPO_4$. There is no statistically significant difference in relative KL^1 intensities between the measured targets. Small differences could be explained by the thick target X-rays' self-absorption [54]. Observed variations in $K\alpha_3$ and $K\alpha_4$ X-ray line relative intensities between Al metal and the measured compounds are much larger and could not be explained with thick target self-absorption, especially since $K\alpha_3$ and $K\alpha_4$ X-ray lines are separated by only about 2 eV. For example, $K\alpha_4/K\alpha_3$ intensity ratios for Al and Al_2O_3 are 0.416 ± 0.026 and 0.638 ± 0.018 respectively (≈ 53% difference).

Table 4: Normalized KL^0, KL^1, KL^2 and KL^3 intensities obtained with 3 MeV ^{4}He excitation and $K\alpha_3$ to $K\alpha_4$ intensity ratios obtained by 3 MeV ^{4}He and 2 MeV proton excitations.

	Al	AlN	Al_2S_3	Al_2O_3	$AlPO_4$
KL^0	0.329 ± 0.004	0.338 ± 0.004	0.330 ± 0.007	0.398 ± 0.012	0.352 ± 0.022
KL^1	0.462 ± 0.005	0.461 ± 0.006	0.469 ± 0.009	0.429 ± 0.012	0.463 ± 0.029
KL^2	0.187 ± 0.008	0.178 ± 0.009	0.176 ± 0.019	0.158 ± 0.025	0.170 ± 0.060
KL^3	0.022 ± 0.004	0.023 ± 0.005	0.024 ± 0.006	0.015 ± 0.005	0.015 ± 0.011
3 MeV He $K\alpha_4/K\alpha_3$	0.381 ± 0.006	0.480 ± 0.006	0.510 ± 0.006	0.520 ± 0.007	0.536 ± 0.013
2 MeV H $K\alpha_4/K\alpha_3$	0.416 ± 0.026	0.579 ± 0.018	0.550 ± 0.021	0.638 ± 0.018	0.720 ± 0.041

Conclusions

The measured Kα x-ray emission spectra of Al and selected compounds after excitation by 2 MeV protons and 3 MeV He ions exhibit statistically relevant variations of the peak position and relative intensities that depend on the chemical state. Energy shifts of $K\alpha_{1,2}$ first moments (M1) are small but measurable and for the measured compounds they show linear decrease with the increase of the calculated effective charge on Al atoms.

Other Kα spectral features that can be extracted from the measured spectra may add additional information into chemical speciation capabilities. Therefore, we investigated the shapes and energy shifts of Al $K\alpha_{1,2}$ multiple ionization satellites (MIS) emitted after proton and helium excitation with 2 and 3 MeV respectively. With 2 MeV proton excitation, the overall relative intensity of all MIS components is at the level of only several percent and only $K\alpha L^1$ can be measured in reasonable time. When measured with 3 MeV He excitation, relative intensity of the $K\alpha L^1$ MIS component is at the level of about 46%, i.e. it makes the dominant contribution to the Kα total intensity. In that case even the low intensity Kα' line is clearly seen in the measured spectra and shows measurable energy shifts which are more than a factor of two larger than the reported $K\alpha_{1,2}$ energy shifts. And similarly, linear dependence of the peak energy shift vs. the effective charge on Al atoms have been observed on $K\alpha L^1$ multiple ionization satellite components Kα' and $K\alpha_4$ measured by 3 MeV He excitation.

In case of the overall KL^1 intensities relative to KL^0, they heavily depend on the type of ions used and their energies. We have not observed statistically significant differences in these relative intensities between the measured targets for both 2 MeV proton and 3 MeV He excitations. Small differences could be explained by the thick target X-rays self-absorption. However, statistically relevant variations in KL^1 components' ($K\alpha_3$ and $K\alpha_4$) relative intensities between Al metal and its compounds have been confirmed. The related shapes of $K\alpha_3$ and $K\alpha_4$ peaks are very similar for both 2 MeV proton and 3 MeV He excitation that confirms large influence of chemical effects. It means that the use of 3 MeV He ions for excitation can be an efficient way to distinguish between the Al and its compounds in investigated microsamples.

Conflicts of interest

There are no conflicts to declare.

Acknowledgements

IBM, SF, AM and MRR acknowledge the support from the Croatian Science Foundation project Hi-REXS [Grant Number 9429].

References

1 A. Meisel, G. Leonhardt, R. Szargan, *X-Ray Spectra and Chemical Binding*, Springer-Verlag (1989)
2 F. de Groot, *Chem. Rev. (Washington, DC, U.S.),* 2001, **101** 1779–1808.
3 G. Hölzer, M. Fritsch, M. Deutsch, J. Härtwig, and E. Förster, *Phys Rev A*, 1997, **56**, 4554-4568.

4 M. Kayhko, M.R.J. Palosaari, M. Laitinen, K. Arstila, I. Maasilta, T. Sajavaara, *X-Ray Spectrometry*, 2018, **47**, 475-483.
5 J. Kawai, M. Ohta, T. Konishi, *Analytical Sciences*, 2005, **21** 865-868.
6 J. Kawai, C. Suzuki, H. Adachi, T. Konishi, Y. Gohshi, *Phys. Rev. B*, 1994, **50**, 11347-11354.
7 J. Kawai, T. Konishi, A. Shimohara, Y. Gohshi, *Spectrochimica Acta B*, 1994, **49**, 725-738.
8 T. Konishi, J. Kawai, M. Fujiwara,T. Kurisaki, H. Wakita,Y. Gohshi, *X-Ray Spectrometry*, 1999, **28**, 470-477.
9 T. Konishi, T. Tsubata, M. Oku, Y.M. Todorov, M. Yoshio, *Analytical Sciences*, 2005, **21**, 861-864.
10 T. Mukoyama, *X-Ray Spectrometry*, 2000, **29**, 413-417.
11 E. Öz, E. Baydaş, Y. Şahin, *Journal of Radioanalytical and Nuclear Chemistry*, 2009, **279**, 529-537.
12 S. Fazinić, I. Božičević Mihalić, M. Kavčič, M. Petric, *Spectrochimica Acta - Part B Atomic Spectroscopy*, 2002, **195**, 106506.
13 U. Bergmann, C. R. Horne, T. J. Collins, J. M. Workman and S. P. Cramer, *Chem. Phys. Lett.*, 1999, **302**, 119–124.
14 J. Badro, J. P. Rueff, G. Vank_o, G. Monaco, G. Fiquet and F. Guyot, *Science*, 2004, **305**, 383–386.
15 S. Fazinić, M. Jakšić, L. Mandić, J. Dobrinić, *Phys. Rev. A*, 2006, **74**, 062501.
16 S. Fazinić, L. Mandić, M. Kavčič, I. Božičević, *Spectrochimica Acta Part B*, 2011, **66**, 461–469.
17 S. Fukushima, T. Kimura, K. Nishida, V. A. Mihai, H. Yoshikawa, M. Kimura, T. Fujii, H. Oohashi, Y. Ito, and M. Yamashita, *Mikrochim. Acta*, 2006, **155**, 141-145.
18 L. Mandić, S. Fazinić,M. Jakšić, *Phys. Rev. A*, 2009, **80**, 042519.
19 D. F. Anagnostopoulos, A. Siozios, and P. Patsalas, *Journal of Applied Physics*, 2018, **123**, 065105.
20 W. L. Baun, D. W. Fischer, *Nature*, 1964, **204**, 642–644.
21 D. W. Fischer and W. L. Baun, *Journal of Applied Physics*, 1965, **36**, 534.
22 D. W. Fischer and W. L. Baun, *Physical Review*, 1966, **145(2)**, 555–560.
23 Eiichi Asada, *Japan J. Appl. Phys.*, 1973, **12**, 1946-1947.
24 P. G. Burkhalter, A. R. Knudson, D. J. Nagel, and K. L. Dunning, *Phys. Rev. A*, 1972, 6, 2093-2101.
25 25. M. Deutsch, *Phys. Rev. A*, 1989, **39**, 1077-1081.
26 M. Keski-Rahkonen, E Mikkola, K Reinikainen and M Lehkonen, *J. Phys. C: Solid State Phys.*, 1985, **18**, 2961-2975.
27 P Suresh, B Seetharami Reddy, T Seshi Reddy, M L N Raju, B V Thirumala Rao, B Mallikarjuna Rao and M V R Murti, *J. Phys. B: At. Mol. Opt. Phys.*, 2000, **33**, 1645–1652.
28 J. Utriainen, M. Linkoaho, E. Rantavuori. T. Aberg, G. Graeffe, *Zeitschrift fur naturforschung Part A – Astrophsik Physik und Physikalische Chemie*, 1968, **A23**, 1178-1182.
29 E. Mikkola, 0. Keski-Rahkonen, J. Lahtinen and K. Reinikainen, *Physica Scripta*, 1983, **28**, 188-192.
30 T. Yamamoto, A. Kanai, K. Hayashi, M. Uda, Nuclear Instruments and Methods in Physics Research B, *1999*, **150**, 60-65.
31 D. S. Urch, *J. Phys. C: Solid St. Phys.*, 1970, **3**, 1275-1291.
32 W. L. Baun and D. W. Fischer, *Journal of Applied Physics*, 1967, **38**, 2092.
33 V. Dutkiewicz, H. Bakhru, and N. Cue, *Phys. Rev. A*, 1976, **13**, 306-311.
34 C. M. Heirwegh, M.Petric, S. Fazinić, M. Kavčič, I. Božičević Mihalić, J. Schneider, I. Zamboni, J. L. Campbell, *Nucl. Instrum. Methods B*, 2018, **428**, 9-16.
35 T. Mukoyama, K. Taniguchi, *Phys. Rev. A*, 1987, **36**, 693-698.
36 W. L. Baun, D. W. Fischer, *Physics Letters*, 1964, **13**, 36–37.
37 F. Hopkins, J. Sokolov, and A. Little, *Phys. Rev. A*, 1976, **14**, 1907-1909.
38 D.J.T. Cureatz, M. Kavčič, M. Petric, K. Isaković, I. Božičević Mihalić, M. Rodriguez Ramos, S. Fazinić, J. L. Campbell, *Spectrochimica Acta Part B: Atomic Spectroscopy*, 2022, **194**, 106483.
39 C. M. Heirwegh, M.Petric, S. Fazinić, M. Kavčič, I. Božičević Mihalić, J. Schneider, I. Zamboni, J. L. Campbell, *Nucl. Instrum. Methods B*, 2022, **428C**, 63034.
40 S. Fazinić, I. Božičević Mihalić, T. Tadić, D. Cosic, M. Jakšić, D. Mudronja, *Nucl. Instr. Meth. B*, 2015, **363**, 61–65.
41 41. I. Božičević Mihalić, S. Fazinić, T. Tadić, D. Cosic and M. Jakšić, *Journal of Analytical Atomic Spectrometry*, 2016, **31**, 2293-2304.
42 42. K. Sato, A. Nishimura, M. Kaino, S. Adachi, *X-Ray Spectrometry*, 2017, **46**, 330-335.
43 S. Lafuerza, A. Carlantuono, M. Retegan, P. Glatzel, *Inorg. Chem.*, 2020, **59**, 12518-12535.
44 R. D. Deslattes, E. G. Kessler, P. Indelicato, L. de Billy, E. Lindroth, J. Anton, *Rev. Mod. Phys.*, 2003, **75**, 35–99.
45 V. F. Demehin, V.P. Sacenko, *Izvestia Akademii Nauk SSSR, Serija Fiziceskaja*, 1967, **T.XXXI No.6**, 907-911.
46 M. Petric and M. Kavčič, *J. Anal. At. Spectrom.*, 2016, **31**, 450-457.
47 R. Alonso Mori, E. Paris, G. Giuli, S. G. Eeckhout, M. Kavčič, M. Žitnik, K. Bučar, L. G. M. Pettersson, and P. Glatzel, *Anal. Chem.*, 2009, 81, 15, 6516–6525.
48 A. Jain, S. Ping Ong, G. Hautier, W. Chen, W. D. Richards, S. Dacek, S. Cholia, D. Gunter, D. Skinner, G. Ceder, and K. A. Persson, *APL Materials*, 2013, **1**, 011002.
49 T. D. Kühne et al., *J. Chem. Phys.*, 2020, **152**, 194103.
50 J. VandeVondele and J. Hutter, *J. Chem. Phys.*, 2007, **127**, 114105.
51 S. Goedecker, M. Teter, and J. Hutter, *Phys. Rev. B*, 1996, **54**, 1703.
52 52. J. P. Perdew, A. Ruzsinszky, G. I. Csonka, O. A. Vydrov, G. E. Scuseria, L. A. Constantin, X. Zhou, and K. Burke, *Phys. Rev. Lett.*, 2009, **100**, 136406.
53 F. L. Hirshfeld, *Theoret. Chim. Acta*, 1977, **44**, 129–138.
54 M. Kavčić, *Nucl. Instr. And Meth. B*, 2020, **477**, 19-22.